JOURNAL OF THE ROYAL SOCIETY Interface

rsif.royalsocietypublishing.org

Research

Cite this article: Gemmell BJ, Adhikari D, Longmire EK. 2014 Volumetric quantification of fluid flow reveals fish's use of hydrodynamic stealth to capture evasive prey. *J. R. Soc. Interface* **11**: 20130880.
http://dx.doi.org/10.1098/rsif.2013.0880

Received: 26 September 2013
Accepted: 23 October 2013

Subject Areas:
biomechanics, environmental science

Keywords:
tomography, predation, animal–fluid interaction, stealth predation, hydrodynamic signals, strain rate

Author for correspondence:
Brad J. Gemmell
e-mail: brad.gemmell@utexas.edu

†Present address: University of Texas, Marine Science Institute, Port Aransas, TX 78373, USA.

Royal Society Publishing

Volumetric quantification of fluid flow reveals fish's use of hydrodynamic stealth to capture evasive prey

Brad J. Gemmell†, Deepak Adhikari and Ellen K. Longmire

Aerospace Engineering and Mechanics, University of Minnesota, Minneapolis, MN 55455, USA

In aquatic ecosystems, predation on zooplankton by fish provides a major pathway for the transfer of energy to higher trophic levels. Copepods are an abundant zooplankton group that sense hydromechanical disturbances produced by approaching predators and respond with rapid escapes. Despite this capability, fish capture copepods with high success. Previous studies have focused on the predatory strike to elucidate details of this interaction. However, these raptorial strikes and resulting suction are only effective at short range. Thus, small fish must closely approach highly sensitive prey without triggering an escape in order for a strike to be successful. We use a new method, high-speed, infrared, tomographic particle image velocimetry, to investigate three-dimensional fluid patterns around predator and prey during approaches. Our results show that at least one planktivorous fish (*Danio rerio*) can control the bow wave in front of the head during the approach and consumption of prey (copepod). This alters hydrodynamic profiles at the location of the copepod such that it is below the threshold required to elicit an escape response. We find this behaviour to be mediated by the generation of suction within the buccopharyngeal cavity, where the velocity into the mouth roughly matches the forward speed of the fish. These results provide insight into how animals modulate aspects of fluid motion around their bodies to overcome escape responses and enhance prey capture.

1. Introduction

Interactions between predator and prey influence the community structure of ecosystems [1]. In aquatic communities, predation on zooplankton by fish is a major trophic pathway [2–4]. However, planktivorous fish must first overcome the highly tuned mechanosensory capabilities of copepods and other zooplankton in order to feed. This interaction is strongly affected by disturbances in the surrounding liquid medium [5–7], so a thorough understanding of the hydrodynamics during predation attempts is critical. For most planktivorous fish, successful feeding is accomplished by rapid suction combined with protrusive jaws [8–10]. Studies have revealed that these flows are strong as a result of substantial low-pressure generation in the buccal cavity [11–13], but exceptionally short lived, lasting only 10–50 ms, and are restricted to an area very close to the mouth [13–17]. Thus, when approaching an individual prey, target fish must approach hydrodynamically sensitive species, for example, copepods, closely, quickly or both before a strike can occur. Copepods are capable of responding to strain rates (sometimes referred to as deformation or shear) as low as 0.5 s^{-1} [18–20]. This poses a problem because fish disrupt fluid when moving towards prey, creating a hydrodynamic disturbance in front of them [5,6,8,21].

It is this disturbance that is sensed by specialized setae of copepods [18,22,23] that can respond to nanometres of fluid displacement [24]. The relative motion of setae leads to neuron depolarization, which triggers an escape response. Copepods are propelled forward by posterior-to-anterior metachronal strokes of the thoracic pereiopods [25], achieving speeds over 500 body lengths per second (BL s^{-1}) [23]. Combined with some of the shortest known response latencies (2–3 ms) this can provide an effective response to predation [23,26].

With respect to swimming performance (BL s^{-1}), copepods outperform the fishes by an order of magnitude, suggesting that an escaping copepod can keep ahead of a pursuing fish that is up to 30 times longer than the copepod itself [23]. Despite the ability of copepods to exhibit some of the shortest response latencies and fastest swimming speeds relative to body size in the animal kingdom, some zooplanktivorous fish have been observed to capture these animals with high efficiency (near 90%) [27,28].

Therefore, when feeding in the water column, fish that employ visually mediated, target-specific, raptorial feeding behaviour must approach close enough to use suction and protrusive jaw movements in order to overcome copepod escape capabilities. Previous studies have provided valuable insight into what occurs during the actual strike [7,27]. However, it must be considered that unless a predator can first closely approach evasive prey without generating an escape response, the strike will be ineffective. Arguably, this initial phase of the interaction, the approach, is at least as important as the strike to the success of prey capture for this feeding mechanism. For other feeding modes such as filter feeding or mass-pulse suction, which engulf large volumes, the approach phase may be less important. It is also possible for fish to use elements of the habitat (e.g. weeds and rocks) to limit escape pathways available to copepods.

The approach phase of the capture of copepods by fish has not been investigated in detail in part owing to the inability to obtain accurate volumetric measurements of fluid patterns produced by fish during interactions with live prey. In this study, we use high-speed, infrared tomographic particle image velocimetry (PIV) to provide volumetric velocity fields around the head of a planktivorous fish (*Danio rerio*) when feeding on a copepod (*Diaptomus leptopus*). Our results show that cruising (non-feeding) swimming produces a principal strain rate profile that extends further from the head and is evenly distributed relative to fish feeding on evasive prey. By contrast, when approaching prey, the strain rate magnitude showed a distinct reduction at the plane of the copepod resulting in a 'stealth' approach that was not detected by prey. We provide a mechanistic explanation for this observation by quantifying a small amount of suction that begins prior to the strike. This 'compensatory suction' [29] acts to reduce hydrodynamic disturbance in front of the fish, at the location of the prey, and allows the fish to get close enough for a successful strike.

2. Material and methods

2.1. Experimental set-up and procedure

Twelve zebrafish (*Da. rerio*; total length: 31 mm (s.d. 2.8)) were housed in a 38 l aquarium at 25°C. The fish were fed a mixed diet of prepared commercial food and live zooplankton, and kept on a 12 L : 12 D cycle. Copepods (*Di. leptopus*; prosome length: 0.7–1.0 mm) were collected from Lake of the Isles, Minneapolis, MN, USA (44°57′6.42″ N 93°18′27.28″ W) using a 0.25 m diameter plankton net (mesh size: 150 µm). They were kept in 20 l aerated containers and used within 24 h of collection. All fish were fed 24 h before experiments commenced to ensure a constant level of initial satiation. Video from only the first suitable feeding attempt was processed.

Experiments were performed in an aquarium of 300 mm (L) × 150 mm (W) × 205 mm (H), filled with water to the depth of 120 mm (figure 1). Water was seeded with 55 µm polyamide (infused with 11% titanium dioxide), neutrally buoyant tracer particles to an approximate density of 200 particles per cubic centimetre. These particles were selected because they are highly reflective at near-infrared wavelengths and are non-toxic to both fish and zooplankton. An Oxford Firefly laser (808 nm; 300 W; 1% duty cycle) was used for illumination. The laser was capable of expanding into a sheet through its internal optical arrangement to the approximate width of the tank with a thickness of 13 mm. The laser was pulsed at 500 Hz, with a pulse duration and energy of 20 µs and 6 mJ, respectively. Mirrors were placed in an inclined manner underneath the tank to reflect the illumination volume, and therefore illuminate particles otherwise obstructed by the shadow of the fish. A near-infrared laser was used because neither fish [30] nor zooplankton [31] are sensitive to this part of the spectrum, which is still within the sensitivity range of CMOS cameras. Near-infrared illumination has been previously used successfully for PIV applications [32,33]. The resulting images were recorded at 500 Hz by four high-speed cameras (Phantom v. 210, Vision Research Inc.), at a resolution of 1280 × 800 pixels. Each camera was fitted with a Scheimpflug adapter to a 200 mm Nikon AF-Micro Nikkor lens, and angled such that the illuminated volume remained in focus across each sensor plane. Fish were transferred to the experimental tank and allowed to acclimate for 15 min before laser illumination and data acquisition. During acquisition, cameras recorded images continuously in a 12 s buffered loop and a post-trigger was applied when the fish was observed executing its predation within the real-time video. After being subjected to an experimental series consisting of two to five prey capture attempts, the fish were placed into a second, identical 38 l aquarium to avoid being used twice. A non-paired comparison was also made of freely swimming fish in the absence of prey. No fish was recorded more than once to avoid pseudo-replication.

2.2. Tomographic PIV and data analysis

The tomographic PIV sequences were processed using the MART algorithm within LaVision DaVis 8.0 software. The details of the procedure (including calibration and preprocessing) are described in [34]. As the presence of a solid object (e.g. the fish) can create artefacts within the measurement volume, a three-dimensional mask is required to prevent these artefacts from impacting calculation of fluid velocity fields. An automated visual hull technique detailed in [35] was applied to mask these volumetric regions and is summarized below.

Fish silhouette images from each of the four cameras were obtained using MATLAB and were imported into DaVis software. The visual hull of the fish was reconstructed by back-projecting the four silhouette images from each camera into an object volume using the Multiplicative Line-of-Sight (MLOS) operation available in DaVis 8.0. Consecutive masked volumes were cross-correlated to obtain a given volumetric velocity field. A multi-pass cross-correlation was then employed. Deviations of the visual hull from the actual shape of the object (figure 2*b*,*c*) are owing to the limited number of cameras and the inability to resolve concavities [35]. However, the visual hull of the fish closely encapsulates the shape of the actual animal, and thus gives an estimate of the location of the object within the field of view. Most importantly, accurate fluid velocity vectors could be determined in regions very close to and surrounding the fish mouth. For suction velocity measurements

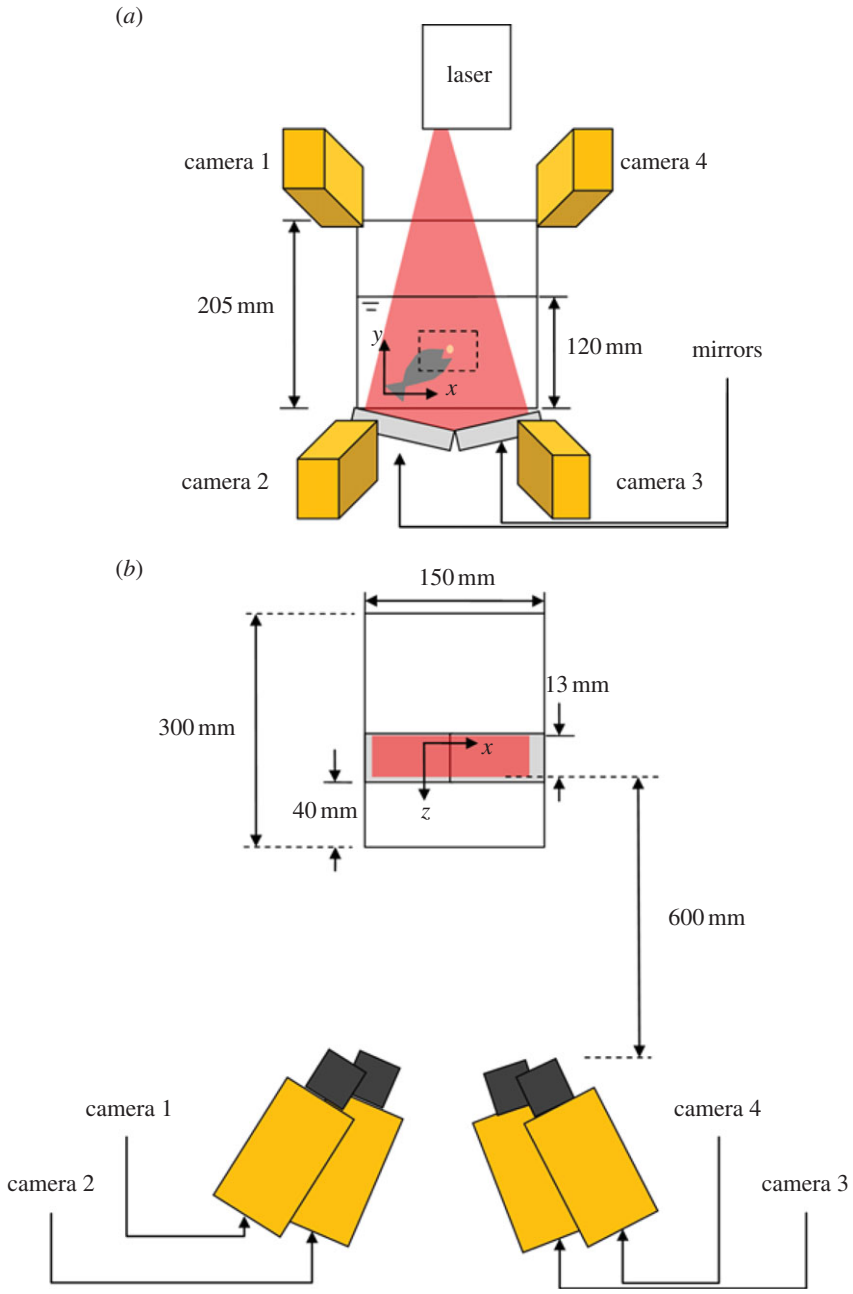

Figure 1. Schematic diagram of experimental set-up, modified from [27]. (*a*) *x*–*y* view. (*b*) *x*–*z* view.

in and around the mouth, particles were manually tracked without the visual hull to allow better near-body resolution.

Calibration, self-calibration and preprocessing steps of tomographic PIV were carried out on a 64-bit Windows PC with four processors and 8 GB of memory. Particle reconstruction and volume correlation, which were more computationally intensive, were processed in parallel on five similar computers. For each time step in a given sequence, vectors were obtained from individual interrogation volumes of dimension 96 × 96 × 96 voxels. Vectors were determined using 75% overlap and resolved on a grid with volume 22.5 × 10.5 × 12 mm.

Copepods are known to respond to velocity gradients in the fluid [5]. Spatial velocity gradients were calculated by applying a central difference method to the three-dimensional Cartesian grids of velocity vectors obtained for each time step. The resulting spatial resolution of each gradient is 1 mm. Quantifying the strength of local strain rates from these gradients is dependent on the coordinate system. As the copepods are aligned at arbitrary angles to the Cartesian coordinates when sensing fluid disturbances, maximum principal strain was used to determine the hydrodynamic disturbance independent of the copepod orientation [36].

The maximum principal strain was calculated by finding the eigenvalues of the symmetric component of the complete velocity gradient tensor (also known as strain rate tensor)

$$e_{ij} = \begin{bmatrix} \dfrac{\partial u}{\partial x} & \dfrac{1}{2}\left(\dfrac{\partial u}{\partial y}+\dfrac{\partial v}{\partial x}\right) & \dfrac{1}{2}\left(\dfrac{\partial u}{\partial z}+\dfrac{\partial w}{\partial x}\right) \\ \dfrac{1}{2}\left(\dfrac{\partial u}{\partial y}+\dfrac{\partial v}{\partial x}\right) & \dfrac{\partial v}{\partial y} & \dfrac{1}{2}\left(\dfrac{\partial v}{\partial z}+\dfrac{\partial w}{\partial y}\right) \\ \dfrac{1}{2}\left(\dfrac{\partial u}{\partial z}+\dfrac{\partial w}{\partial x}\right) & \dfrac{1}{2}\left(\dfrac{\partial v}{\partial z}+\dfrac{\partial w}{\partial y}\right) & \dfrac{\partial w}{\partial z} \end{bmatrix},$$

where u, v, w are the velocity components in the orthonormal x, y, z directions, respectively, and

$$\det(e_{ij} - \lambda_k \delta_{ij}) = 0.$$

In the above equation, det refers to the determinant of the tensor, δ_{ij} is the Kronecker delta tensor and λ_k ($k = 1, 2, 3$)

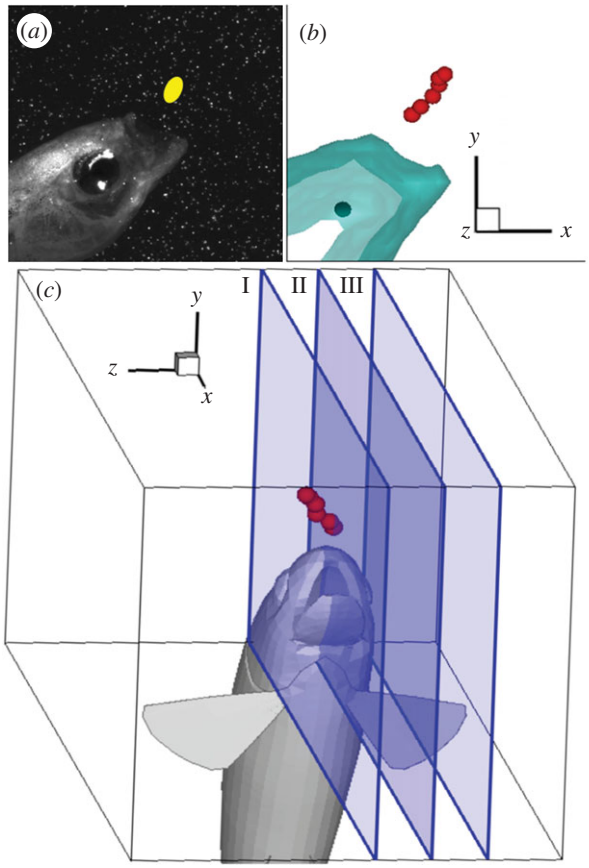

Figure 2. Selected instance of the zebrafish *Da. rerio* performing a feeding strike on the copepod *Di. leptopus*. (*a*) Raw image from one of the four high-speed cameras. The location of the copepod is shown by a yellow oval for clarity. (*b*) The image from (*a*) with the visual hull mask applied to allow accurate fluid vector determination. Red spheres show the path of the escaping copepod before ingestion over $t = 0-14$ ms. (*c*) Simulated fish showing the locations of vertical planes I, II and III corresponding with the principal strain rate profiles in figure 2. Planes I and III are drawn at the edge of the fish's head, whereas plane II is drawn at the initial location of the copepod.

represent the eigenvalues, or principal strain rates. The maximum principal strain rate is then obtained as $\lambda_{max} = \max(|\lambda_1|, |\lambda_2|, |\lambda_3|)$.

The motion tracking procedures for both predator and prey are described in detail in [34] and consist of two steps: (i) locating a point on the organism in the images and (ii) triangulating the point into a three-dimensional location based on two or more camera images. The uncertainty of predator and prey location in the images was 1 pixel. This translates to a location uncertainty of 0.02 mm, and a velocity uncertainty of 0.028 m s^{-1} in each of the *x*-, *y*- and *z*-components for both predator and prey. Velocities of suction flow during the fish's approach to a copepod were estimated by manually tracking particles in ImageJ v. 1.46 software.

Statistical comparisons of swimming speed and suction velocity was performed using Student's *t*-test. Comparisons of mean principal strain rates were performed using a one-way analysis of variance (ANOVA). Data were checked for normality using a Shapiro–Wilk test.

3. Results

We measured the mean cruising (non-predatory) swimming speed of zebrafish to be 44.2 mm s^{-1} (s.d. 4.5, $n = 10$) which is nominally faster than the fish speed during approaches to copepod prey (30.1 mm s^{-1}, s.d. 6.0, $n = 8$). Approach speed of zebrafish to non-evasive prey at 35.6 mm s^{-1} (s.d. 6.2, $n = 9$) was also greater than approach speed to evasive prey but not significantly different ($p = 0.10$, *t*-test). Flow fields surrounding each swimming behaviour were reconstructed. Figure 2 shows a raw image of the zebrafish feeding on a copepod and the corresponding three-dimensional visual hull mask. Three *xy* planes (figure 2*c* I, II and III) are used to illustrate volumetric variations in strain rate (s^{-1}) created by the fish; one plane down the median sagittal plane which closely corresponds to the plane of the copepod, and one on either edge of the fish head. The spacing between planes is 2.4 mm. It should be noted that the red dots marking the copepod swimming path are overlaid by the strain coloration in the bottom two panels of column III in figure 3. During the final stages of the approach on evasive prey (figure 3*a*,*b*), it is observed that: (i) strain rate created by the bow wave of the moving fish is comparatively low and (ii) there is a pronounced reduction in strain rate at the fish sagittal plane, which coincides with the plane of the copepod (figure 3; column II and figure 4) compared with the strain rate values at the edges of the head (figures 2 and 3). During the initial phase of the strike, the fish begins to accelerate rapidly towards the copepod resulting in a large increase in strain rate (figure 3*c*) and a breakdown of the reduced strain rate zone. As the strike progresses, suction is created by the fish to aid in prey capture. This creates a second observable reduction in strain rate at the sagittal plane of the head as suction roughly matches the fluid velocity created by the fish as it lunges forward (panel II; figure 3*d*,*e*). The copepod begins to escape at 4 ms (figure 3*c*). By contrast, the hydrodynamic (strain rate) profile in front of the fish extends further and shows no reduction in strain rate at the sagittal plane of the head (where prey is normally positioned) during normal swimming (figure 5).

The main difference between approaching prey and routine swimming observed from the high-speed recordings is that during predatory behaviour, the mouth opens 94 ms (s.d. 14) before the strike commences during the final stages of the approach as the fish nears the copepod. This occurred in 100% of observed interactions with prey species. The mouth was observed to open more than 0.4 mm during the approach compared with ≈2.5 mm at the point the copepod is ingested. During routine swimming, the mouth of *Da. rerio* was not measurably open from a side profile. By contrast, the presence of suction created by the mouth was observed and measured well in advance of the predatory strike. Suction velocities were significantly different ($p < 0.001$, *t*-test) between approaches and strikes. Suction velocity averaged 30 mm s^{-1} at the time of mouth opening and increased to approximately 75 mm s^{-1} as water entered the buccal cavity (figure 6). This prestrike suction during the approach corresponds to the observed reduction in strain rate at the plane of the prey.

The rapid, lunging strikes of *Da. rerio* towards the copepod *Di. leptopus* occurred at distances between 2.1 and 2.5 mm from the copepod. The prestrike suction began at distances of approximately 5 mm from the copepod. Copepods were unresponsive to approaches by *Da. rerio* but responded with rapid escape jumps to the initial strike. This initial phase consists of the completion of the C-start position [37] where the body is positioned to allow quick burst swimming. The initial acceleration creates a comparatively strong hydrodynamic disturbance that is detectable by copepods (figure 2*c*). The

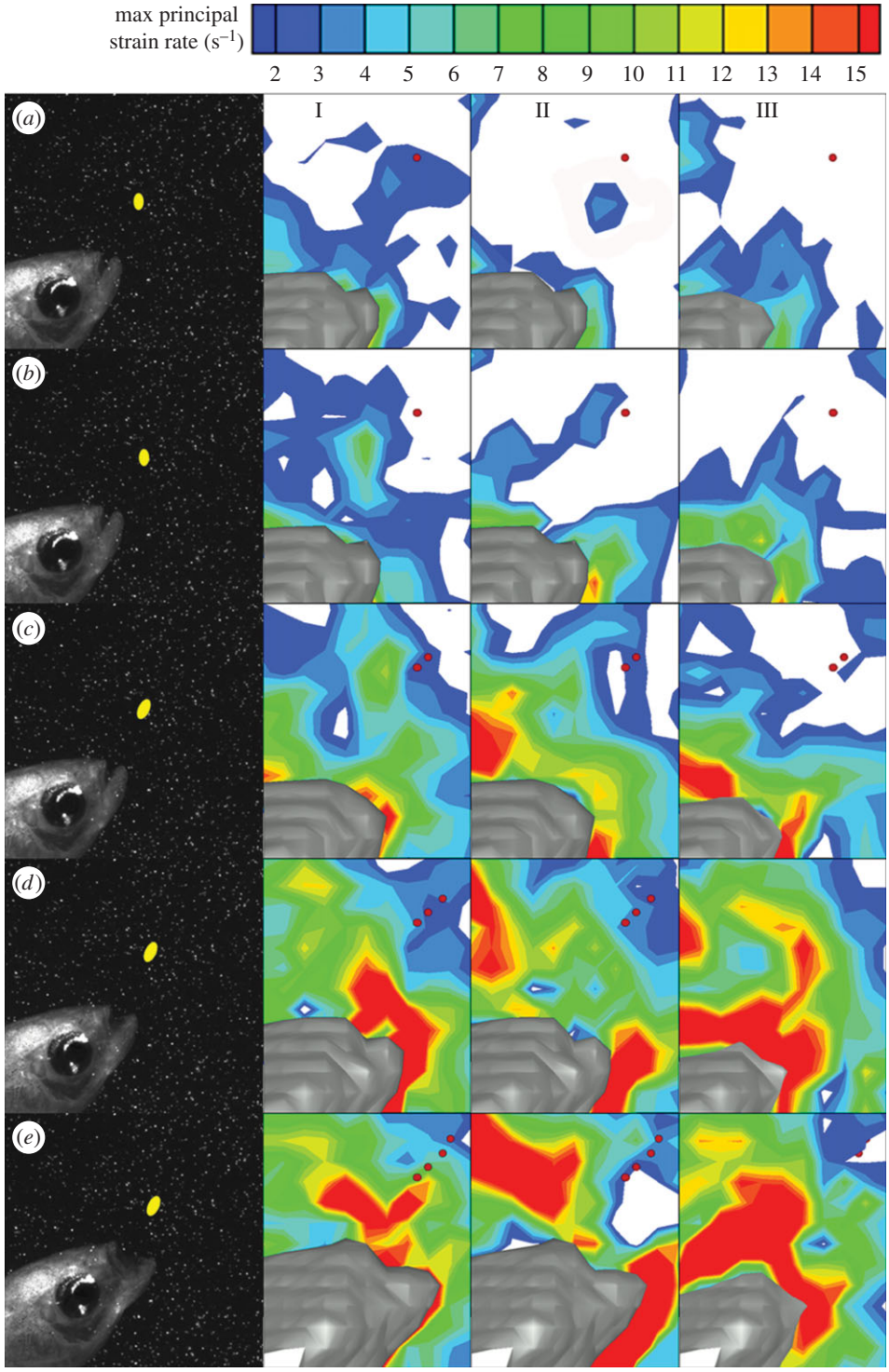

Figure 3. Strain rate contours just prior to and during the initial phase of the feeding strike. Profiles are drawn at three locations across the head that correspond to planes I–III in figure 1. (*a*,*b*) Strain rates are reduced at plane II, which represents the location of the copepod. (*c*–*e*) As the strike begins strain rates increase sharply and extend further from the head as the copepod senses the disturbance and begins to mount an escape jump. Note that strong suction can also act to reduce the hydrodynamic disturbance of the rapid approach of the fish at the central plane in panel (*e*) II.

resulting escape behaviour by copepods produced average velocities of 280 mm s^{-1} (416 mm s^{-1} maximum) compared with fish strike velocities of 250 mm s^{-1} (404 mm s^{-1} maximum).

Principal strain rate magnitude at the region where feeding strikes occur (average prey location prior to strike) is significantly greater ($p < 0.001$, ANOVA) during both routine swimming and feeding on non-evasive food than during feeding approaches on evasive prey. Strike speed is also significantly greater ($p < 0.001$) during feeding attempts on evasive prey.

4. Discussion

Evolutionary pressure has driven copepods to become so sensitive to hydrodynamic disturbances that from a purely morphological standpoint it appears unlikely that zooplanktivorous fish can approach close enough and quickly enough to use effective short-range strikes to capture their prey. Using high-speed, infrared tomographic PIV, we are able to demonstrate that zooplanktivorous fish exhibit a behavioural solution to this problem. This volumetric method shows that

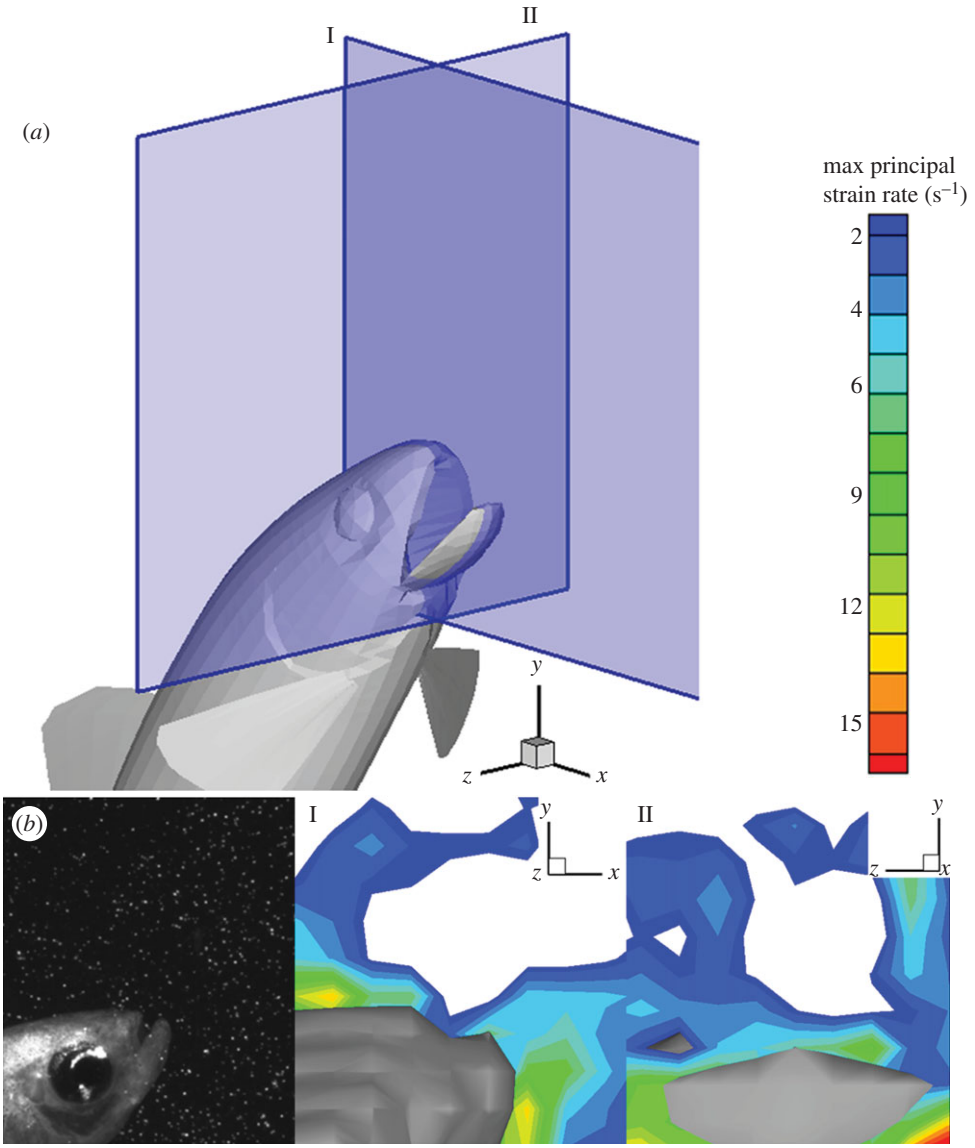

Figure 4. Perpendicular planes at the opening of the mouth showing the spatial variation in principal strain rate. (*a*) Locations of planes shown in (*b*). Planes I and II transect the location of the copepod. (*b*) Raw image of the zebrafish approaching a copepod with two reconstructed views of the principal strain rate profiles which correspond to I and II in panel (*a*), and to the middle plane (II) in figure 2*c*.

by creating a small amount of suction at the mouth during the approach, fluid disturbance is reduced at the copepod location. Figure 5 shows the comparison between routine swimming and a predatory approach of similar velocities. When performing routine swimming, the principal strain rate profile at the sagittal plane of the fish's head (where copepod is generally positioned before a strike) exceeds detection limits of most copepods more than or equal to 3 mm in front of the head. However, the zebrafish can modulate and reduce the strain rate distribution in front of the head to create a zone of 'hydrodynamic stealth' when approaching evasive prey at nearly identical speeds as routine swimming (figures 2–4).

Is the 'stealth zone' required for prey capture? Why do not the fish simply strike from a greater distance (3+ mm)? The answer probably has to do with the fact that the strike from 3 mm instead of 2 mm would take 1.5 times as long to reach the location of the copepod. At the fish's mean strike speed of 250 mm s^{-1} this amounts to only an additional 4 ms, but for prey species whose escape response latency is only 2–4 ms, it would probably result in significant changes to capture success. We find this 'stealth' zone to be created by suction from opening the mouth less than 0.4 mm, 94 ms (s.d. 14) before the strike commences. This process begins to occur approximately 5 mm away from the prey, where fluid disturbance from routine swimming is still undetectable to the copepod. The strength of suction is important to successfully approach evasive prey. Suction that is too weak will not effectively mask the hydrodynamic signal of the fish and suction that is too strong will act to create fluid strain with the principal vector in the opposite direction. At the opening of the mouth, suction velocities are found to approximately match the forward swimming velocity and local suction velocity increases when entering the buccal cavity (figure 5). This allows the formation of a pocket of low principal strain rate (figure 3), and the fish approaches the copepod so as to position the prey within this pocket.

Consider that, during the strike, *Da. rerio* exhibits a mean velocity of 244 mm s^{-1}, whereas the copepod, *Di. leptopus* exhibits a mean escape velocity of 256 mm s^{-1}. Therefore, the fish would be unable to make up ground on the copepod, which is consistent with the estimate given by [23]. Thus,

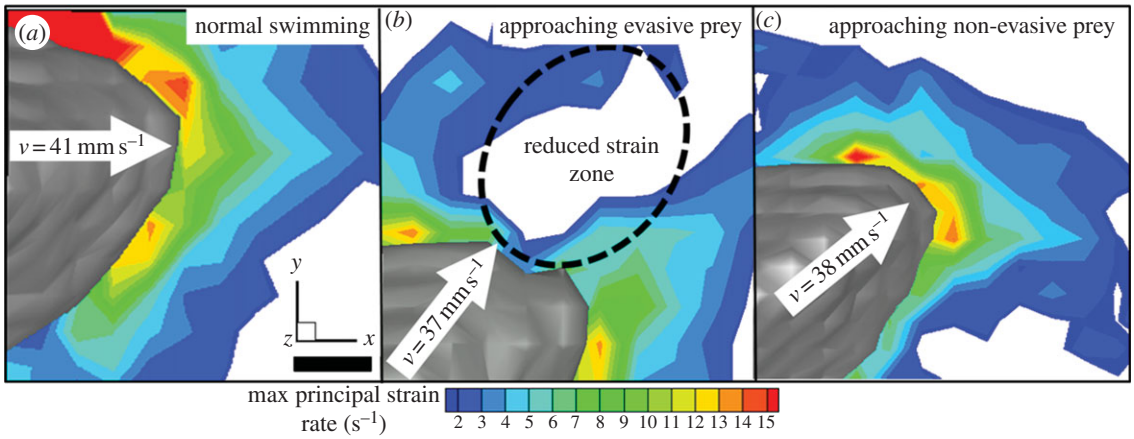

Figure 5. Comparison of representative strain rate profiles from: (*a*) normal (non-predatory swimming); (*b*) predatory approach to evasive prey represented in figure 2*b* II; and (*c*) approach to non-evasive prey. Scale bar, 1 mm.

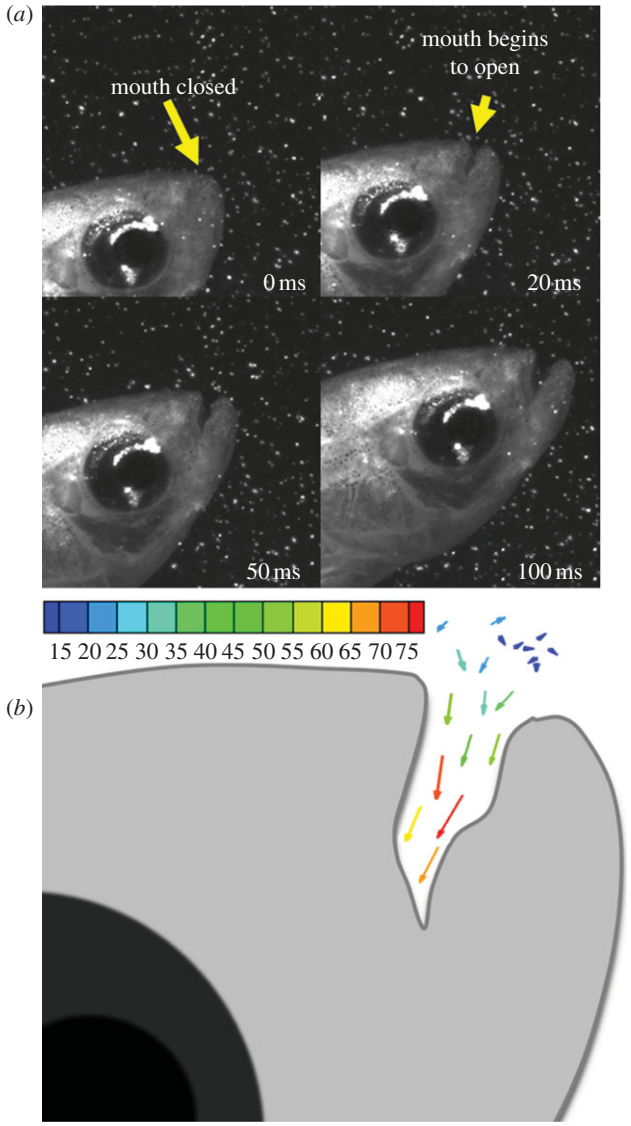

Figure 6. Mechanistic explanation for the presence of reduced strain rates during approaches to evasive prey. (*a*) Time series of the approach beginning when the fish approaches to within 5 mm of the copepod. (*b*) Result of tracking individual tracer particles at 2 ms intervals over the 100 ms approach duration represented in panel (*a*), confirming the presence of suction as the fish nears the copepod. Scale is millimetres per second.

striking from a distance (more than 3 mm, in the case of *Da. rerio*) required to approach a copepod without behavioural strain rate modification is likely to result in failure of the predator for several reasons: (i) suction to entrain prey works only at close range, so increasing the distance from prey will reduce the effectiveness of this mechanism; (ii) the fish cannot make up the extra distance with a speed advantage over its prey and (iii) the copepod is unlikely to escape in the identical direction as the fish strike. Escapes perpendicular to the fish strike path will allow copepods to exit the strike zone most quickly. Thus, the greater the strike distance of the fish, the greater the likelihood that the copepod will have time to safely exit the strike zone as the fish were not observed to alter the strike path once it has been initiated.

Is the formation of a low-strain region specific for evasive prey? We observed no evidence of the mouth opening prior to initiation of the strike when fish were fed on a prepared flake diet or less-evasive zooplankton (*Daphnia* sp.). When the principal strain magnitude profiles are investigated around the head of *Da. rerio* feeding on non-evasive food, the result is similar to that of routine swimming where a large bow wave is observed in front of the head (figure 5). This is in contrast to the behaviour of fish feeding on evasive copepods (figures 3 and 4), where strain rate in the strike region is significantly reduced ($p < 0.001$, ANOVA) relative to both routine swimming and feeding on non-evasive food. This is despite there being no significant difference ($p = 0.10$) in approach speed. Interestingly, strike speed is significantly greater ($p < 0.001$) during feeding attempts on evasive prey. Thus, it appears this mechanism for reducing strain in the strike region is adaptive for evasive prey and can be actively regulated by fish (as can strike speed). Additionally, when evasive copepods were presented to fish previously fed only non-evasive food, initial strikes were unsuccessful and copepods frequently responded prior to a strike. However, behavioural adjustments resulting in success occurred quickly (more than 1 min). These results also imply a cost for behaviourally reducing strain in the strike region. By abandoning this behaviour in the absence of evasive prey, it is likely that more food can be ingested as approach speed can be higher and additional time required to generate the low-strain region and position prey within it are not needed.

The controlled use of suction to reduce hydrodynamic signals may be a widespread solution among visually mediated, raptorial feeders. Earlier studies [29,38,39], which investigate head and jaw movements of turtles feeding on evasive prey (fish), investigated and identified what is termed 'compensatory suction'. Here, the biomechanics of head movement during feeding suggested a preliminary suction to compensate for head and body movements. This movement corresponds to the preparatory phase of the strike [40]. In fish, Ferry-Graham *et al*. [13] found that the bow wave extended less than 10% of the body length and that peak flows were located away from the mouth. However, the link between head kinematics and hydrodynamic signals available to prey was missing. The use of high-speed, volumetric PIV allows us to elucidate the hydrodynamic function of compensatory suction and demonstrate the ability to reduce fluid strain in a planktivorous fish.

It is important to note that the effect of turbulence on this predator–prey interaction was not considered. However, we know that turbulence affects the interaction of fish and their planktonic prey [41]. Copepods are less capable of responding to hydrodynamic signals in the presence of turbulence [42,43]. Therefore, it may be the case that behaviourally mediated compensatory suction is most useful/predominant in calm environments where turbulence is low and prey sensitivity to hydrodynamic disturbances is near the detection limit. Another factor not considered is repeat capture attempts and/or prey fatigue. It has been suggested that both habituation and fatigue can affect copepod escape response [44], so in nature copepods may still be captured effectively through predatory mechanisms that produce a detectable signal. However, if reducing strain rates during an approach leads to capture in fewer attempts, it may still be advantageous and selected for.

The head morphology of many planktivorous fish will produce a hydrodynamic disturbance immediately in front of it that appears relatively uniform in cross section as it approaches the prey (figure 5*a*). A potential flow model shows that the extent of the perturbed fluid volume in front of the fish forebody will increase linearly with the approach speed. Therefore, a trade-off exists: the faster the fish moves towards the copepod, the further away the copepod will be able to detect the fish's presence. Conversely, approaching at a speed that is slow enough to keep fluid strain rates below 0.5–3.0 s^{-1} to successfully get within a few millimetres of a copepod will require very low speeds and significantly increase approach time. Given that copepods display routine (non-escape) swimming speeds of several millimetres per second [45,46] this will increase the likelihood that the mean prey swimming speed can outpace the predator, and thus keep the copepod out of the strike zone.

Biological flows are inherently three dimensional. The use of high-speed volumetric imaging has already provided new insights into animal–fluid interactions [33,47,48] that were not possible with planar techniques. In this study, the use of high-speed, volumetric tomographic imaging with infrared illumination allows tracking of both fish and copepod locations while simultaneously quantifying how fish predators can behaviourally mask hydrodynamic signals to copepods. This provides insight into a trophic interaction that is responsible for moving vast amounts of energy throughout aquatic food webs. The detection and quantification of a mechanism that aids in the capture of evasive prey helps to explain how a common, but short-range, feeding mechanism can be successfully deployed on highly sensitive, evasive prey.

Funding statement. This work was supported by a grant from the National Science Foundation, USA to E.K.L. (NSF IDBR-0852875).

References

1. Turner AM, Mittelbach GG. 1990 Predator avoidance and community structure: interactions among piscivores, planktivores, and plankton. *Ecology* **71**, 2241–2254. (doi:10.2307/1938636)
2. Kerfoot WC, Sih A. 1987 *Predation: direct and indirect impacts on aquatic communities*. Hanover, NH: University Press of New England.
3. Aksnes DL, Nejstgaard J, Sœdberg E, Sørnes T. 2004 Optical control of fish and zooplankton populations. *Limnol. Oceanogr.* **49**, 233–238. (doi:10.4319/lo.2004.49.1.0233)
4. O'brien W. 1987 Planktivory by freshwater fish: thrust and parry in the pelagia. In *Predation: direct and indirect impacts on aquatic communities* (eds C Kerfoot, A Sih), pp. 3–16. Hanover, NH: University Press of New England.
5. Kiorboe T, Visser AW. 1999 Predator and prey perception in copepods due to hydromechanical signals. *Mar. Ecol. Prog. Ser.* **179**, 81–95. (doi:10.3354/meps179081)
6. Visser AW. 2001 Hydromechanical signals in the plankton. *Mar. Ecol. Prog. Ser.* **222**, 1–24. (doi:10.3354/meps222001)
7. Wainwright PC, Day SW. 2007 The forces exerted by aquatic suction feeders on their prey. *J. R. Soc. Interface* **4**, 553–560. (doi:10.1098/rsif.2006.0197)
8. Holzman R, Wainwright PC. 2009 How to surprise a copepod: strike kinematics reduce hydrodynamic disturbance and increase stealth of suction-feeding fish. *Limnol. Oceanogr.* **54**, 2201–2212. (doi:10.4319/lo.2009.54.6.2201)
9. Drenner RW, Strickler JR, O'Brien WJ. 1978 Capture probability: the role of zooplankter escape in the selective feeding of planktivorous fish. *J. Fish. Board Can.* **35**, 1370–1373. (doi:10.1139/f78-215)
10. Weihs D. 1980 Hydrodynamics of suction feeding of fish in motion. *J. Fish Biol.* **16**, 425–433. (doi:10.1111/j.1095-8649.1980.tb03720.x)
11. Sanford CP, Wainwright PC. 2002 Use of sonomicrometry demonstrates the link between prey capture kinematics and suction pressure in largemouth bass. *J. Exp. Biol.* **205**, 3445–3457.
12. Lowry D, Motta PJ. 2008 Relative importance of growth and behaviour to elasmobranch suction-feeding performance over early ontogeny. *J. R. Soc. Interface* **5**, 641–652. (doi:10.1098/rsif.2007.1189)
13. Ferry-Graham LA, Wainwright PC, Lauder GV. 2003 Quantification of flow during suction feeding in bluegill sunfish. *Zoology* **106**, 159–168. (doi:10.1078/0944-2006-00110)
14. Day SW, Higham TE, Cheer AY, Wainwright PC. 2005 Spatial and temporal patterns of water flow generated by suction-feeding bluegill sunfish *Lepomis macrochirus* resolved by particle image velocimetry. *J. Exp. Biol.* **208**, 2661–2671. (doi:10.1242/jeb.01708)
15. Holzman R, Collar DC, Day SW, Bishop KL, Wainwright PC. 2008 Scaling of suction-induced flows in bluegill: morphological and kinematic predictors for the ontogeny of feeding performance. *J. Exp. Biol.* **211**, 2658–2668. (doi:10.1242/jeb.018853)
16. Van Wassenbergh S, Aerts P. 2009 Aquatic suction feeding dynamics: insights from computational modelling. *J. R. Soc. Interface* **6**, 149–158. (doi:10.1098/rsif.2008.0311)
17. Holzman R, Day SW, Wainwright PC. 2007 Timing is everything: coordination of strike kinematics affects the force exerted by suction feeding fish on attached prey. *J. Exp. Biol.* **210**, 3328–3336. (doi:10.1242/jeb.008292)

18. Kiørboe T, Saiz E, Visser A. 1999 Hydrodynamic signal perception in the copepod *Acartia tonsa*. *Mar. Ecol. Prog. Ser.* **179**, 97–111. (doi:10.3354/meps179097)
19. Waggett RJ, Buskey EJ. 2007 Copepod escape behavior in non-turbulent and turbulent hydrodynamic regimes. *Mar. Ecol. Prog. Ser.* **334**, 193–198. (doi:10.3354/meps334193)
20. Fields DM, Yen J. 1997 The escape behavior of marine copepods in response to a quantifiable fluid mechanical disturbance. *J. Plankton Res.* **19**, 1289–1304. (doi:10.1093/plankt/19.9.1289)
21. Vogel S. 1996 *Life in moving fluids: the physical biology of flow*. Princeton, NJ: Princeton University Press.
22. Strickler JR, Bal AK. 1973 Setae of the first antennae of the copepod *Cyclops scutifer* (Sars): their structure and importance. *Proc. Natl Acad. Sci. USA* **70**, 2656–2659. (doi:10.1073/pnas.70.9.2656)
23. Buskey E, Lenz P, Hartline D. 2002 Escape behavior of planktonic copepods in response to hydrodynamic disturbances: high speed video analysis. *Mar. Ecol. Prog. Ser.* **235**, 135–146. (doi:10.3354/meps235135)
24. Yen J, Lenz PH, Gassie DV, Hartline DK. 1992 Mechanoreception in marine copepods: electrophysiological studies on the first antennae. *J. Plankton Res.* **14**, 495–512. (doi:10.1093/plankt/14.4.495)
25. Strickler J. 1985 Feeding currents in calanoid copepods: two new hypotheses. *Physiol. Adapt. Mar. Anim. Symp. Soc. Exp. Biol.* **39**, 459–485.
26. Waggett RJ, Buskey EJ. 2007 Calanoid copepod escape behavior in response to a visual predator. *Mar. Biol.* **150**, 599–607. (doi:10.1007/s00227-006-0384-3)
27. Coughlin DJ, Strickler JR. 1990 Zooplankton capture by a coral reef fish: an adaptive response to evasive prey. *Environ. Biol. Fish.* **29**, 35–42. (doi:10.1007/BF00000566)
28. Gemmell BJ, Buskey EJ. 2011 The transition from nauplii to copepodites: susceptibility of developing copepods to fish predators. *J. Plankton Res.* **33**, 1773–1777. (doi:10.1093/plankt/fbr066)
29. Van Damme J, Aerts P. 1997 Kinematics and functional morphology of aquatic feeding in Australian snake-necked turtles (Pleurodira; *Chelodina*). *J. Morphol* **233**, 113–125. (doi:10.1002/(SICI)1097-4687(199708)233:2<113::AID-JMOR3>3.0.CO;2-7)
30. Lythgoe J, Partridge J. 1989 Visual pigments and the acquisition of visual information. *J. Exp. Biol.* **146**, 1–20.
31. Stearns D, Forward R. 1984 Copepod photobehavior in a simulated natural light environment and its relation to nocturnal vertical migration. *Mar. Biol.* **82**, 91–100. (doi:10.1007/BF00392767)
32. Epps BP, Techet AH. 2007 Impulse generated during unsteady maneuvering of swimming fish. *Exp. Fluids* **43**, 691–700. (doi:10.1007/s00348-007-0401-4)
33. Murphy D, Webster D, Yen J. 2012 A high-speed tomographic PIV system for measuring zooplanktonic flow. *Limnol. Oceanogr. Methods* **10**, 1096–1112. (doi:10.4319/lom.2012.10.1096)
34. Adhikari D, Longmire EK. 2013 Infrared tomographic PIV and 3D motion tracking system applied to aquatic predator–prey interaction. *Meas. Sci. Technol.* **24**, 024011. (doi:10.1088/0957-0233/24/2/024011)
35. Adhikari D, Longmire E. 2012 Visual hull method for tomographic PIV measurement of flow around moving objects. *Exp. Fluids* **53**, 943–964. (doi:10.1007/s00348-012-1338-9)
36. Catton KB, Webster DR, Yen J. 2012 The effect of fluid viscosity, habitat temperature, and body size on the flow disturbance of *Euchaeta*. *Limnol. Oceanogr. Fluids Environ.* **2**, 80–92. (doi:10.1215/21573689-1894514)
37. Domenici P, Blake R. 1997 The kinematics and performance of fish fast-start swimming. *J. Exp. Biol.* **200**, 1165–1178.
38. Summers AP, Darouian KF, Richmond AM, Brainerd EL. 1998 Kinematics of aquatic and terrestrial prey capture in *Terrapene carolina*, with implications for the evolution of feeding in cryptodire turtles. *J. Exp. Zool.* **281**, 280–287. (doi:10.1002/(SICI)1097-010X(19980701)281:4<280::AID-JEZ4>3.0.CO;2-K)
39. Lauder GV, Prendergast T. 1992 Kinematics of aquatic prey capture in the snapping turtle *Chelydra serpentina*. *J. Exp. Biol.* **164**, 55–78. (doi:10.1016/0022-0981(92)90136-X)
40. Lauder GV, Reilly SM. 1996 The mechanistic bases of behavioral evolution: a multivariate analysis of musculoskeletal function. In *Phylogenies and the comparative method in animal behavior*, pp. 104–137.
41. MacKenzie BR, Miller TJ, Cyr S, Leggett WC. 1994 Evidence for a dome-shaped relationship between turbulence and larval fish ingestion rates. *Limnol. Oceanogr.* **39**, 1790–1799. (doi:10.4319/lo.1994.39.8.1790)
42. Gilbert OM, Buskey EJ. 2005 Turbulence decreases the hydrodynamic predator sensing ability of the calanoid copepod *Acartia tonsa*. *J. Plankton Res.* **27**, 1067–1071. (doi:10.1093/plankt/fbi066)
43. Robinson H, Finelli CM, Buskey EJ. 2007 The turbulent life of copepods: effects of water flow over a coral reef on their ability to detect and evade predators. *Mar. Ecol. Prog. Ser.* **349**, 171–181. (doi:10.3354/meps07123)
44. Hwang J-S, Strickler R. 2001 Can copepods differentiate prey from predator hydromechanically? *Zool. Stud.* **40**, 1–6.
45. Van Duren LA, Videler JJ. 1995 Swimming behaviour of developmental stages of the calanoid copepod *Temora longicornis* at different food concentrations. *Mar. Ecol. Prog. Ser.* **126**, 153–161. (doi:10.3354/meps126153)
46. Kjellerup S, Kiørboe T. 2012 Prey detection in a cruising copepod. *Biol. Lett.* **8**, 438–441. (doi:10.1098/rsbl.2011.1073)
47. Flammang BE, Lauder GV, Troolin DR, Strand TE. 2011 Volumetric imaging of fish locomotion. *Biol. Lett.* **7**, 695–698. (doi:10.1098/rsbl.2011.0282)
48. Flammang BE, Lauder GV, Troolin DR, Strand T. 2011 Volumetric imaging of shark tail hydrodynamics reveals a three-dimensional dual-ring vortex wake structure. *Proc. R. Soc. B* **278**, 3670–3678. (doi:10.1098/rspb.2011.0489)